E

"Miscellaneous"

In this chapter other, less obvious applications are examined. In paragraph E1 the underwater use of a Microflown is discussed. This application can be of use for underwater source localisation such as passive sonar. Such equipment is used to listen if there are another submarines and also to find out where they might be located. The Microflowns that are used as Hydrodflowns do not yet have the proper noise figures. Theoretically they should operate properly, so research must put in to find out what went wrong and how to make it right. Contradictory to air-acoustics particle velocity microphones do exist in underwater-acoustics.

Another application that is used for source localisation is an infrasound array. The array is made in such way that it is sensitive to detect the origin of very low frequency noise sources such as planes flying through the sound barrier, meteors entering the earth's atmosphere,

volcano explosions, nuclear explosions etc. A sixteen-element array with an aperture of 1.5 km is used to detect these phenomena. Nowadays microbarographs are used and in part E2 the use of Microflown is investigated.

The Microflown orginates from a mass flow sensor. It is therefore not surprising that it is very sensitive to DC flow. Paragraph E3 is disclosing some information about this subject.

A complete other application is the use of a Microflown as a level-sensor. The operation principle is still based on the temperature difference of two identical heaters but now this difference is caused by buoyancy of air; no external flow is present. First experiments show an adequate sensitivity though high accuracy operation is hampered by thermal drift.

Although the Microflown is a modulator type of sensor, it is able to produce sound. The sound that is generated by the Microflown is caused by temperature variations of the sensor-wires. The temperature variations cause a pressure fluctuation that can be perceived as sound.

E1 THE HYDROFLOWN

Introduction

The Microflown is a particle velocity sensor that is based on the principles of a mass flow sensor. These sensors operate both in air as in various liquids. In this chapter the use of a Microflown is investigated as a particle velocity sensor for underwater measurements.

Since water is electrically conducting and the boiling point is about 100°C, the Microflown is put in a package that is filled with oil and acoustically transparent. This oil has almost the same acoustic properties as water but is not electrically conducting and has a higher boiling point than water.

Underwater acoustic values

The specific acoustic impedance at a point in a sound field is defined as the ratio of the complex amplitude of an individual frequency component of sound pressure, at that point, to the complex amplitude of the associated component of particle velocity. The particle velocity is observed in one direction, noted as its complex amplitude *u*.

$$Z_s = \frac{p}{u} [\, Ns / m^3 \,] \tag{208}$$

Under free field conditions the specific acoustic impedance equals the product of the density ρ of the medium and the speed of sound c in the medium. The speed of sound in air is 340m/s and the density of air is 1.3kgm^{-3}, the specific acoustic impedance in air equals 440Nsm^{-3} (or Ray). The density of water equals 1000kgm^{-3} and the speed of sound in water 1500m s^{-1}. The specific acoustic impedance in water equals 1500kNsm^{-3}. The specific acoustic impedance is therefore 3400 times higher in water than in air.

The associated particle velocity component of a sound pressure wave in water is 3400 times lower than that in air.

	Air	Water
Speed of sound [m/s]	340	1500
Density [kgm^{-3}]	1.3	1000
Acoustic Impedance [Ns/m^{-3}]	440	1500.000
Particle velocity due to 1Pa [mm/s]	2.3	0.000667
Particle displacement 1Pa & 1kHz [nm]	370	0.11
Specific heat [kJ/kg K]	1	4.18
Thermal conductivity [W/mK]	0.041	0.6

The lowest underwater noise level at 1kHz equals 160μPa, the associated particle displacement 18×10^{-15} m. For comparison, the atoms in water 1×10^{-10} m apart from each other.

The reference sound pressure level that is used for underwater acoustics is 1μPa (in air this is 20μPa).

A standing wave tube is used for calibration. Contradictory to air-acoustics, in underwater-acoustics the sound pressure is zero at the end of the tube (in air-acoustics the particle velocity is zero at the end of the tube, see chapter AV "*Calibration methods*"). This is because the mass of water is much higher than air: the water can vibrate freely at the end of the tube causing the velocity to have any value and the sound pressure to be zero. The measurement results clearly show this discrepancy.

Due to the density of water, an air bubble in water can be compared to vacuum in air (a sound pressure minimum) and it is very difficult to create a "hard wall" i.e. a boundary at which the particle velocity is zero.

Expected underwater sensitivity of a Microflown

Since the Microflown is based on a mass flow sensor, see [1], the sensitivity is proportional to the product of the density of the fluid and the specific heat. Water is 770 times dense than air. The specific heat of water is 4.2 times higher than air. The product of the density of the fluid and the specific heat is 3200 times higher in water than in air and the associated particle velocity component of a sound wave in water is 3400 times lower than in air. And therefore:

The sensitivity of the Microflown related to sound pressure in water is expected almost the same as in air.

The relation between the operating temperature and the power dissipation is a function of the thermal conductivity of the fluid. The thermal conductivity of air is 15 times larger than in air. The power dissipation can therefore be chosen much times higher in water to reach the operation same temperature as in air. The signal to noise ratio is dependent on the square root of the power dissipation so this will be higher in water than in air. However, because of the boiling point of oil, the temperature cannot reach the same height as in air. So, thus the sensitivity must be expected to be lower in water than in air.

Influence of boiling point of the fluid

Fig. 142 shows the relative resistance increase due to the increased temperature of the Microflown as result of an increase in power dissipation. Due to the higher thermal conductivity of oil, the temperature-increase is higher in air than in oil.

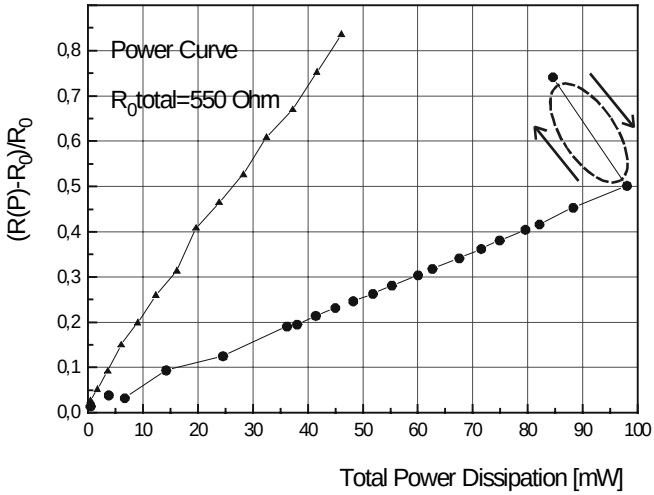

Fig. 142: (Power Curve). The temperature of the sensors increases with rising power dissipation. In air the temperature will rise more than in a fluid.

Hydroflown

In oil at 275°C something is happening: the oil starts to decompose at 200°C and to burn at 300°C. At a value of $(R(P)-R_0)/R_0=0.5$ the temperature of the wires becomes 275°C. This is believed to be caused by an oil-gas bubble that, due to the high local temperature, is created in between both the wires. Due to the presence of a gas bubble the heat conductance drops and the temperature increases rapidly to 400°C. Consequently the resistance of the wires is rising and the power dissipation decreases ($P=U^2/R$). Due to the lower power dissipation the temperature will drop to 275°C and the gas bubble disappears, the resistance drops with the temperature and therefore the power dissipation increases: the process is repeated. This effect has a period time of about one minute.

Because of the changed temperature and power dissipation, and the acoustic impedance change due to the gas bubble at place of the Microflown, the sensitivity of the Microflown is strongly influenced, see Fig. 143.

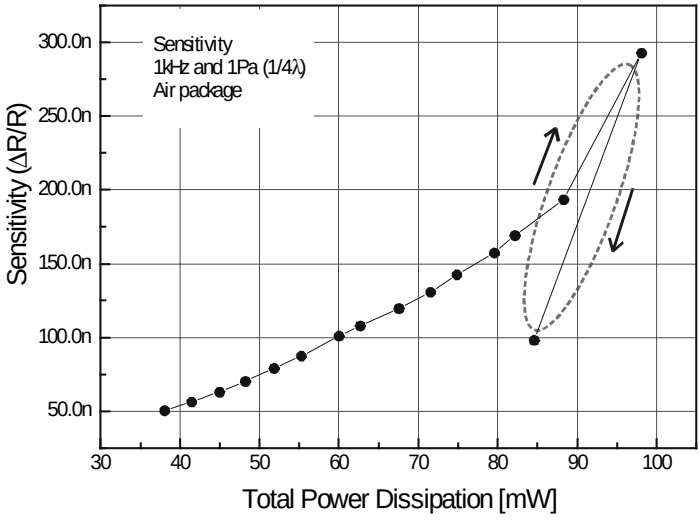

Fig. 143: The sensitivity measured in a standing wave tank.

Influence of the mass of the fluid

The mass of the fluid is high compared with that in air-acoustics. The mass of the sensor therefore becomes relevant: if it is comparable to the fluid the complete microphone moves with the fluid and therefore no sensitivity is observed (in that case the relative velocity of the Microflown is zero). Therefore the Microflown was glued to a piece of metal with a high mass.

Noise levels

The noise of an acoustic sensor is an important figure, it limits the measurements for low signals. The lowest sound levels that can be expected are signals that are above the noise level of the sea itself.

The dominant noise source that is observed in the sea is generated by the wind. These wind induced noise levels are given by the so-called *Knudsen spectra* (see also Fig. 150):

Sea State	Noise $dB(ref.1\mu Pa)/\sqrt{Hz}$	Wind Speed (knods)
0	$44-17Log_{10} f_{kHz}$	<1
0.5	$50-17Log_{10} f_{kHz}$	1-4
1	$55-17Log_{10} f_{kHz}$	4-6
2	$62-17Log_{10} f_{kHz}$	6-11
3	$65-17Log_{10} f_{kHz}$	11-16
4	$67-17Log_{10} f_{kHz}$	
6	$70-17Log_{10} f_{kHz}$	28-33

The Microflown is powered in the constant voltage mode. The noise that is generated by the Microflown is caused by the thermal noise of the sensors. It is given by (see chapter 4):

$$V_{noise} = \sqrt{2kTR} \quad \left[V/\sqrt{Hz}\right] \tag{209}$$

The value of the resistors is in the order of 400Ω and the temperature is in the order of 500K. The noise output of the Microflown will be:

$$V_{noise} = \sqrt{2\times 1.38\cdot 10^{-23}\times 500\times 400} = 2.5nV/\sqrt{Hz} \tag{210}$$

The output Voltage of the Microflown can be calculated by:

$$V_{out} = \tfrac{1}{2} E \frac{\Delta R}{R} \tag{211}$$

E being the supply voltage and ΔR/R the sensitivity of the Microflown. For lower temperatures, the expected sensitivity in air of a Microflown is about 10‰ (re. 1m/s), see chapter 4. The relative differential resistance variation due to 1Pa in air is 25×10^{-6}. At a supply voltage of about 7V the output voltage due to 1Pa in air is 175µV (a sensitivity of 175µV/Pa equals to –195dB re. 1V/µPa). If used underwater the output due to 1Pa is expected to be almost the same. If this sensitivity is obtained under water the signal to noise level will be 97dB/√Hz, and per √Hz a sound pressure level of 23dB (re. 1µPa) could be measured.

Measurement set-up

The measurement set up consists of a standing wave tube filled with oil. The end of the tube is an open end (pressure zero). At this end, there should be a particle velocity maximum at this end (contradictory to the standing wave tube in air).

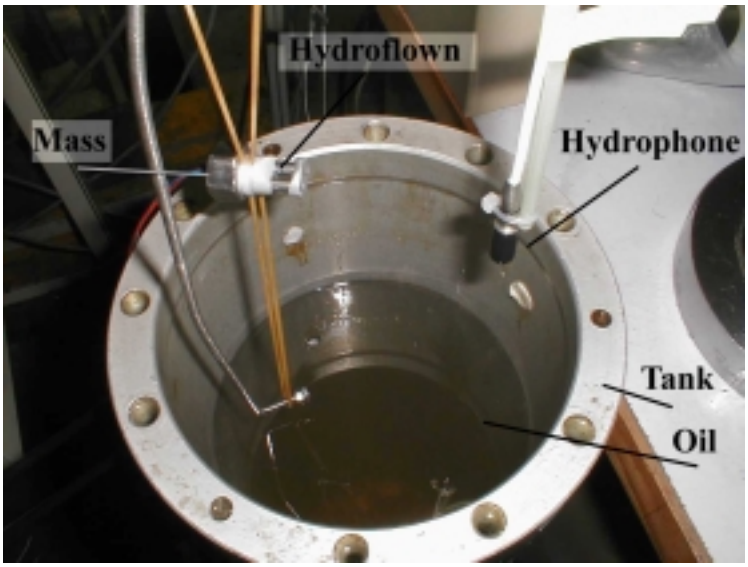

Fig. 144: Picture of the measurement set up. Here the Microflown is packaged.

The pressure sensor that is used is a B&K type 1803 hydrophone and has a sensitivity of –211.6dB (re. 1V/µPa) or 26.3µV/Pa.

The oil that is used has a density of 970kg/m^3 and the speed of sound in oil is 940m/s. The specific acoustic impedance in oil therefore equals 912kNs/m^{-3}.

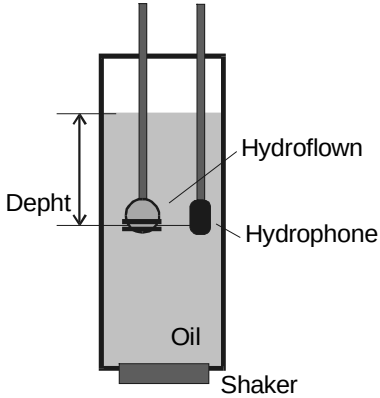

Fig. 145: Measurement set-up. Oil in a standing wave tank.

The associated particle velocity component of a sound pressure wave in oil therefore is 2070 times lower than in air.

	Water	Oil
Speed of sound [m/s]	1500	940
Density [kgm^{-3}]	1000	970
Acoustic Impedance [Ns/m^{-3}]	1500.000	911.000
Particle velocity due to 1Pa [nm/s]	667	1096
Particle displacement 1Pa & 1kHz [nm]	0.11	0.17
Specific heat [kJ/kgK]	1	1.7

The specific heat of oil is 1.7 times higher than air and oil is 746 times denser than air. The Microflown in oil should be 1270 times more sensitive in oil than in air.

The sensitivity of the Microflown related to the sound pressure in oil is expected to be about 1.6 times less than in air.

Hydroflown

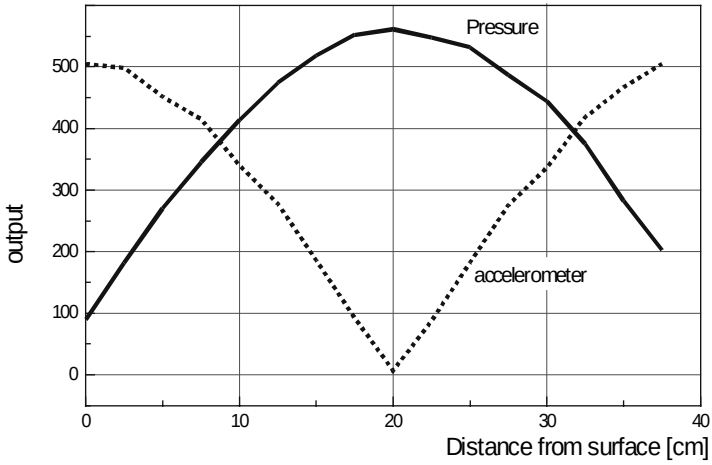

Fig. 146: Reference measurement: sound pressure and acceleration (d*u/dt*) depending on the place in the standing wave tube.

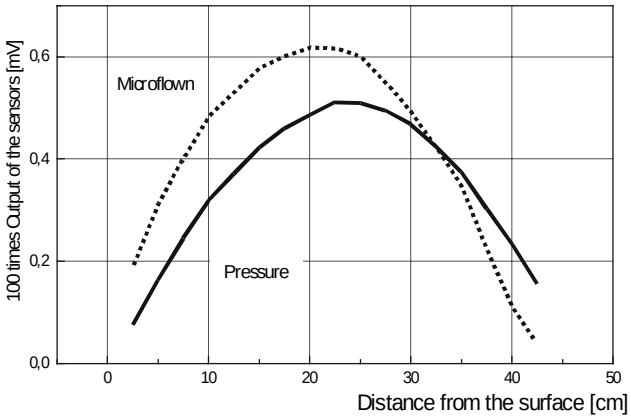

Fig. 147: Measurement of the packaged Microflown. It is (almost, the minima are not exactly on the same location) sensitive for pressure and the sensitivity is high: a maximum of –1.3dB relative to the hydrophone: noise level below sea state zero. It is also directional.

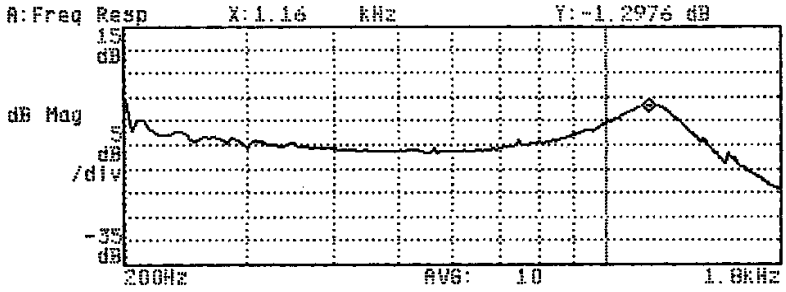

Fig. 148: Measurement of the packaged Microflown. Reference is the hypdrophone at the same height in the tank.

The results that are displayed in Fig. 147 and Fig. 148 show that a Microflown that is packaged has a sensitivity of -223dB re. 1V/µPa up to 1kHz and a sort of resonance peak of +10dB at 1.16kHz.

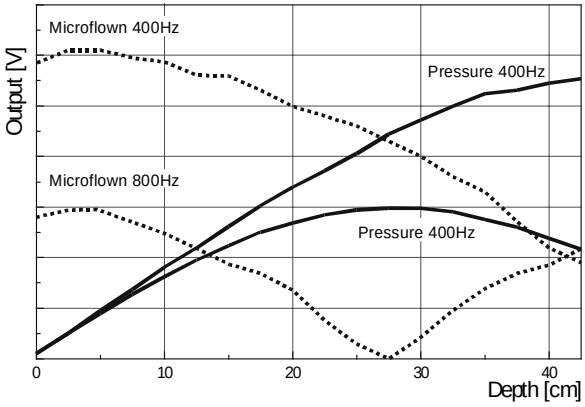

Fig. 149: Response of the non-packaged Microflown and hydrophone as function of the depth in the tank: now the Microflown acts as a velocity sensor.

The packaged Microflown is sensitive to pressure in stead of particle velocity and a resonance peak. This would suggest that it has something to do with a Helmholtz packaged, see chapter D1: "*The sound pressure Microflown*". The packaged Microflown is however directional (figure of eight, plus sign), this is suggest particle velocity sensitivity. We could not find a possible agreement of these results. Since the standing wave tube clearly shows a sound pressure sensitivity of the packaged Microflown, the package was abandoned.

Hydroflown

The results without a package clearly show a particle velocity sensitivity as can be observed in Fig. 149. The sensitivity however was considerable lower: -258dBV/Pa. Furthermore the resonance peak was not observed anymore. The (and the signal to noise ratio) however is 46dB lower without a package. (Sensitivity thus is -258dBV/Pa)

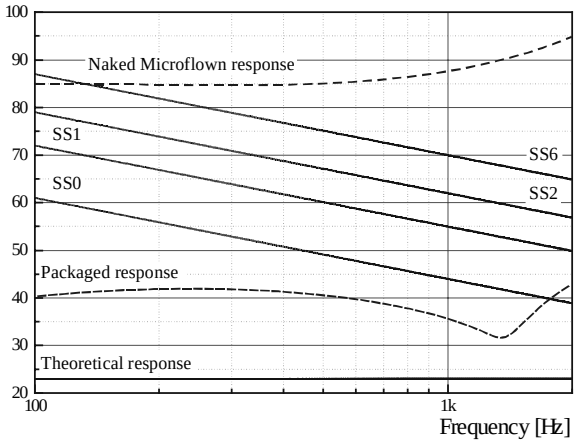

Fig. 150: Response of the non-packaged Microflown, the packaged Microflown and theoretical response.

Conclusion

The Microflown can be used as a sensor for underwater detection of the particle velocity. To be usable it should be attached to a high mass. The sensitivity however is very low. This is believed to be caused by the movements of the wires with the fluid. The lateral rejection is about 10dB.

If packaged the sensitivity rises about 40dB. Such sensitivity would make a good performing sensor, however due to the packaging it is become sensitive to the pressure in stead of the particle velocity.

References

[1] T.S.J. Lammerink et al, “Micro Liquid Flow Sensor,” *Sensors and Actuators A*, pp.37-38, 45-50, (1993).

E2 INFRASOUND EVENT ARRAY

The Seismology Division of the Royal Netherlands Meteorological Institute (KNMI) has build up expertise in infrasound measurements by investigating low frequency events in order to distinguish between seismic and sonic events. KNMI operates, amongst others, a sixteen element microbarometer array with an aperture of 1.5 km, the Deelen Infrasound Array (DIA). Sonic booms and events of Comprehensive Test Ban Treaty (CTBT) interest are detected an identified within the frequency range of 500 seconds up to 40 Hertz. Recently, KNMI and Microflown Technologies B.V. started a collaboration concerning infrasound measurements. This chapter reports experiments with the Microflown for infrasound detection and is based on [61].

Introduction

Recently, the significance of infrasound measurements has been established in the Comprehensive Test Ban Treaty (CTBT) as a technique to detect and identify possible nuclear explosions. For this purpose a world-wide network of 60 infrasound arrays is presently being constructed. KNMI operates since 1999 an experimental array in the Netherlands. The Deelen Infrasound Array (DIA) consist of in house developed micro-barometers, based on a differential pressure sensor. Detailed array response calculations have resulted in a omni-directional sensitive array configuration. Efficiently discrimination between infrasound events and noise, is done with a detector based on Fisher statistics. Characteristic values like apparent sound velocity and azimuth, can be derived. Inclusion of the data of two other small arrays (aperture of 100 meters) results in an accurate event location, through cross-bearing, and origin time.

Pressure variations consist of compression and dilatation with a certain frequency. The frequency is resolved by the Microflown through the frequency of the induced temperature differences. The Microflown has advantages, which are tested together with KNMI for infrasound applications, compared to micro-barometers and pressure microphones. The Microflown has no moving parts, which make it very reliable.

Resonances do not occur. Given its underlying thermal principle, the self-drying Microflown is moisture resistant and it is made from inert materials (platinum, silicon) so that no corrosion problems have to be e expected. All materials used sustain high temperatures. The Microflown is developed at the University of Twente and commercialised by Microflown Technologies B.V.

The Deelen Infrasound Array

In general, an array consists of a number of instruments which is, through its layout, able to detect signals and localise the incoming direction of energy. The array configuration controls the resolution of the array. An optimal array is equally sensitive to all infrasonic signals, independent of their incoming angle and direction. Array design and calculations are based on signal coherency. The optimal array is capable of homogeneously sampling the surrounding atmosphere [62]. Fig. 151 displays the layout of the 16 micro-barometers and corresponding response. To each micro-barometer six porous hoses are connected in star configuration to reduce noise. The circular response implies an optimal array.

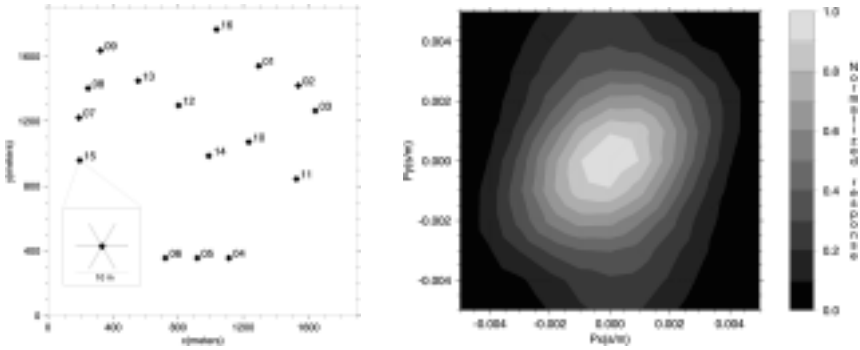

Fig. 151: Deelen Infrasound Array (DIA), instrument lay-out on the left and array response on the right.

Infrasonic signals

Sources of infrasound emit pressure fluctuations between 500s and 40Hz. Examples of infrasonic sources are: planes flying through the sound barrier, meteors entering the earth's atmosphere, volcano explosions, nuclear explosions etc. Wind causes noise within the same frequency band, between 1 and 10 Hz. Fig. 152 shows two examples of infrasound record by the 16 micro-barometers. A high frequent sonic boom on the left and a lower frequent meteor detection at the right. Two packages of incoming energy can be distinguished in the meteor recording. The delay time of the secondary arrival of 50 seconds and its lower frequency contents (with respect to the first arrival) indicate a probable thermospheric reflection [64].

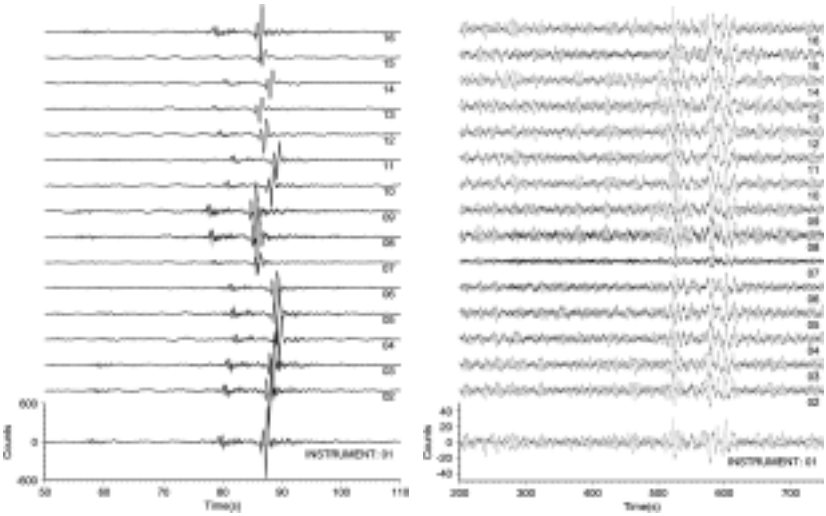

Fig. 152: Examples of infrasonic signals, a sonic boom on the left and meteor recording on the right.

Data processing: frequency slowness analysis

As proposed by [63], data processing at KNMI is performed based on frequency slowness, being the inverse of apparent sound velocity, analysis combined with Fisher statistics. Frequency domain processing, in stead of conventional time domain processing, enables the development of detection tools by making use phase, amplitude, frequency and coherency characteristics. Fisher values are a measure of the signal coherency. An infrasonic wave that travels over the array coherently will add-up to high Fisher values. Uncorrelated signals, like wind, will result in low Fisher values, typically between 0 and 4. Mathematically the Fisher value represents a signal to noise ratio scaled with the number of instruments minus one.

Fig. 153 shows the result of the frequency domain processing. All frames have the same time axis. The top frame displays the best beam or the sum of all signals. The lower three frames represent three parameters each. Frequency and time axes are for all frames the same, but in each frame a third parameter is plotted (as grey coloured contour). Coherency is plotted in the middle frame as Fisher value. Resolved event characteristic: azimuth and velocity are plotted in the lower two frames. Azimuth is defined as the angle from which the energy comes with respect to the north. The resolved velocity is the apparent sound velocity or the projection of the sound velocity on the horizontal.

As follows from the Fisher values, coherent energy is present throughout the recording between 0 and 3Hz. This can be seen as the presence of light to dark grey colours between 0 and 3Hz. The major arrival after 85 seconds results in the highest Fisher values of 160, due to its high amplitude and preserved waveform while travelling over the array.

The coherency of the signal is also reflected when evaluating the incoming angle of the energy. The band of light grey colours between 0Hz and 3Hz roughly indicate that the source is located to the north-west of the array, i.e. an azimuth of 330 degrees.

The apparent velocity in the lower frame seems less well resolved. A mix of all grey colours appears between 0Hz and 3Hz. The lobe of light grey between 2Hz and 3Hz around 85 seconds correspond to reasonable apparent sound velocities of 350m/s. To obtain exact values for the apparent sound velocity and azimuth, a detailed analysis is done.

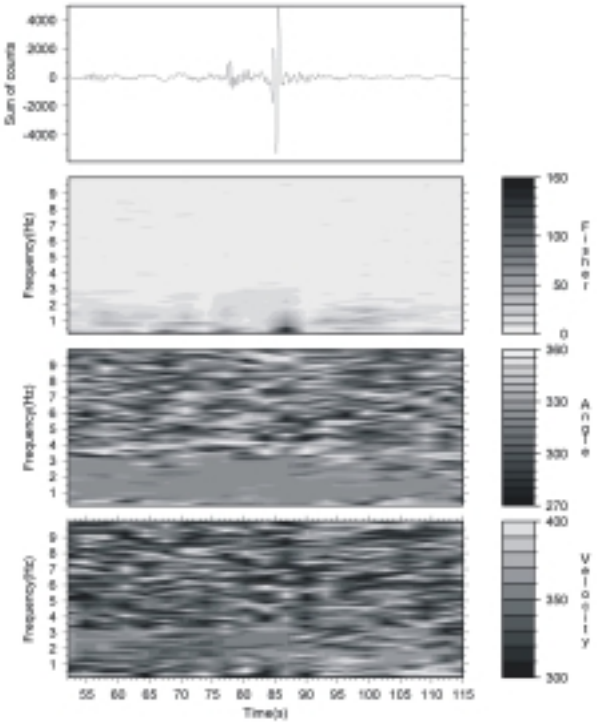

Fig. 153: Best beam (top frame), coherency or Fisher value (middle frame) and resolved angle or azimuth and apparent sound velocity in the lower two frames for the sonic boom (signals displayed left in Figure 2).

Results from detailed frequency slowness analyses of the sonic boom, are displayed Fig. 154. Frequency slowness power can be interpreted as a shifted array response due to the phase differences of the signal travelling over the array. The highest values of the fp-power correspond to the value for slowness for which the signal characteristics are best resolved. In Fig. 154 the maximum coherent energy around 0.5Hz at 85 seconds is exactly located. The white slowness vector resolves an apparent sound velocity of 350m/s, which is proportional to length. The source is located to the north-west of the array by the angle with respect to the North of the slowness vector, being 324 degrees.

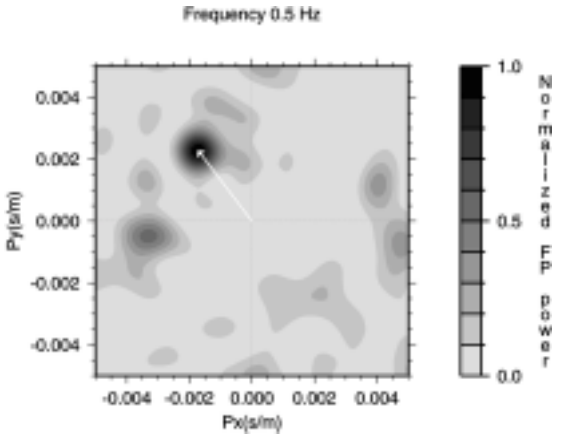

Fig. 154: Frequency-slowness power plots. The white slowness vector denotes the resolved apparent sound velocity of 350m/s by its length and resolved azimuth of 324 degr by its angle with respect to the North.

The KNMI Micro-barometer

When developing an infrasound sensor one can either choose to make a microphone low frequent or a barograph high frequent. KNMI choose the latter approach for amongst others robustness with respect to the field applications. Fig. 155 shows the in house developed micro-barometer based on a differential pressure sensor. The pressure fluctuations are measured with respect to the backing volume. Doing so, one would also measure very low frequent meteorological pressure variations. Therefore, a thin capillary is included within the backing volume, as a leak. Through its acoustical resistance, the capillary controls the low frequency cut-off of the micro-barometer, being 500 seconds.

The Microflown without a (wind) noise reducing mounting

With the use of a 12” loudspeaker a 20Hz sine tone was generated. The distance between the loudspeaker and the transducers was 50cm. Signals and noise levels of the micro-barometer and the Microflown were compared. Furthermore the on- and off axis output of the Microflown was measured. The output signals of the Microflown and the micro-barometer were respectively 85mV and 20mV, their noise levels about

0.2mV and 2mV. A rough estimation would be that that the signal to noise ratio of the Microflown is about 30dB higher than the micro-barometer. The lateral reduction at 20Hz was measured to be 40dB. The measurement was performed by rotating the Microflown and in a normal room.

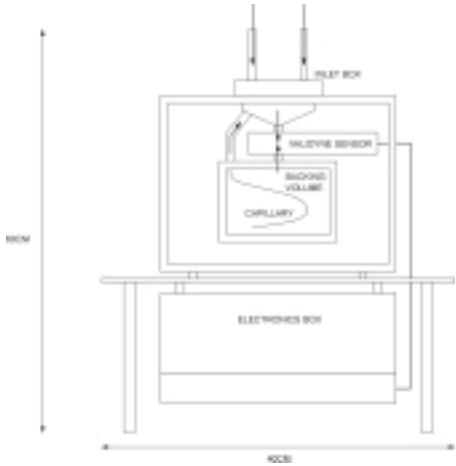

Fig. 155: Schematic drawing of the KNMI micro-barometer based on a differential pressure sensor.

The Microflown with a (wind) noise reducing mounting

At one input of the Microflown a closed rigid tube was mounted and at the other a flexible tube was mounted. A sound pressure wave would deform the flexible tube and not the rigid one, inducing a particle velocity inside the mounting.

This way of noise reducing makes the set up sensitive to sound pressure in stead of particle velocity; the directivity properties of the Microflown are therefore lost. The rigid tube will act as backing volume. We used a volume of 0.6l. We expect the system to detect lower frequencies if the backing volume is enlarged. Opening the door of the lab resulted in signals shown in Fig. 156. Despite the difference in transducing, the general trend of the signal is similar. The “noise” seen on the Microflown is due to electronic interference, it is not selfnoise. The

flexible tube is used as a pressure to particle displacement converter. We expect a higher sensitivity and a better noise reduction when the length of the tube is increased.

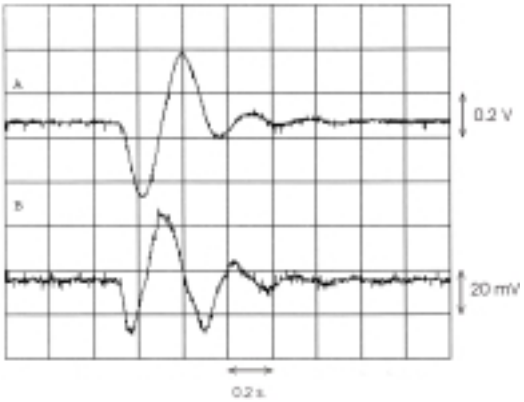

Fig. 156: The measured signals of a micro-barometer (A) and a Microflown (B) as result of an atmospheric distortion in a room with a volume of 144m^3.

Microflown and microphone experiments in the field

The Microflown has been tested in the field. For this purpose, the Microflown was incorporated in an existing array of six microphones (see Fig. 157). Wind reduction for the Microflown was achieved with foam.

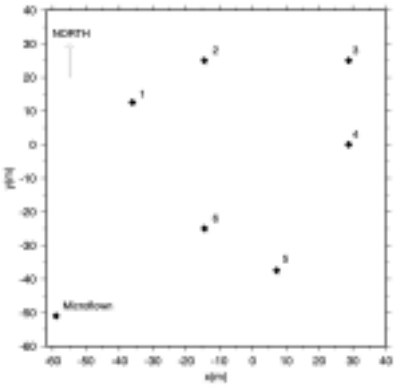

Fig. 157: Microflown within a six-element microphone array.

Fig. 158 shows the performance of the different instruments. A sonic boom coherently travelled over the array. Although exactly locating the energy is not the purpose of this experiment, clearly the energy is coming from the north-west since the Microflown and microphone number 1 were the first to detect the signal. The highly sensitive Microflown, measuring particle velocity, shows a good performance with respect to the microphones. The Microflown trace seems more noisy, this is mainly due to the primitive wind reduction. Currently, research concerns the construction of a robust instrument and noise reduction for durable operation in the field.

Infrasound array

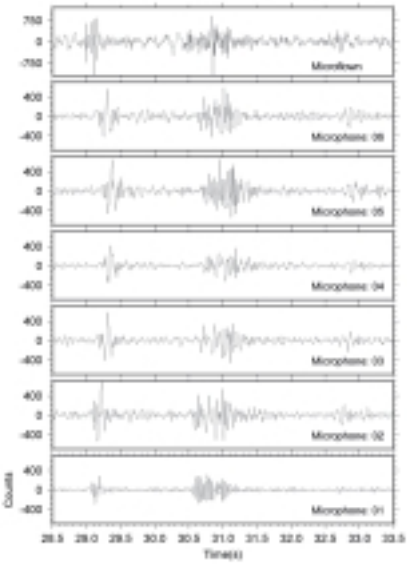

Fig. 158: Recording at approximately 200 km distance of a plane flying through the sound barrier above North Sea.

Conclusion

The Deelen Infrasound Array is capable of detecting and localising infrasound. Identification of sources of infrasound is achieved by using frequency-slowness analysis combined with Fisher statistics. Experiments with the Microflown have shown promising results, as low noise, directional and particle velocity sensor. Proven durability in the field, developments to obtain a proper low frequency cut-off and wind noise reduction will allow the Microflown to be a highly competitive infrasound sensor.

References

[61] L.G. Evers, H-E de Bree, H.W. Haak, A.A Koers, The Deelen infrasound array for recording sonic booms and events of CTBT interest, Aalborg may 2000.

[62] H.W. Haak, An acoustical array for subsonic signals, Tech. Rep. WR96-03, KNMI, De Bilt, the Netherlands, 1996.

[63] E. Smart and E.A.Flinn, Fast frequency-wavenumber analysis and Fisher signal detection in real-time infrasonic array data processing, Geoph. J. R. astr. Soc., volume 26, 1971, pp. 279-284

[64] Garcés et al., Traveltimes for infrasonic waves propagating in a stratified atmosphere. Geoph. J. Int. Volume 135, 1998, pp. 255-263

E3 DC FLOW SENSOR

An extended mass-flow sensor is presented here. Apart from the magnitude of the flow, as an add-on to the traditional anemometer, this sensor also measures the direction of the flow. This is of interest for the flow sensor market in general, and in particular for the safety monitoring of low over-pressure systems like surgery and cleanrooms where the risk of reverse flow needs to be avoided at all times. It detects the smallest amount of gas-flow, down to approximately 100 μm/s airflow up to high flow levels of 20m/s. The response time is in the order of milliseconds. In the discussion a constant temperature principle is presented that allows the Microflown to operate up to 20m/s.

Introduction

For static low flow applications the mass-flow sensor is used commonly [1]. However, for higher flow rates this sensor becomes non-linear and non-invertable (i.e. two possible air velocities have the same output value). For dynamic low flow purposes the Microflown has proven its applicability in the form of a particle velocity microphone [2]. Again, this sensor is not able to detect high level flows. For higher (static and dynamic) flow-rates the anemometer has been widely used [3]. The information about the direction of the flow however can not be found from the output signal of an anemometer. Moreover, the usability of this sensor seems to be limited to the higher flow rates.

Here a combination of all these sensing principles is presented: a bi-directional flow sensor with a large dynamic range. In contrast to regular mass flow sensors the Microflown consists of two wires [4]. The differential and average temperature of both wires is measured by monitoring their electrical resistance. In this way for a mass-flow principle containing the information on the direction of the flow is derived for the low-flow region. For the higher flow-region the anemometer principle is used. The directionality (plus or minus) is detected by means of the differential output.

Theory

The theory on the two flow sensing principles will be treated briefly. First only one heated wire will be observed: the anemometer [2]. An electrical current heats this wire with a constant power. After that, the total signal is found by taking the summation (anemometer) and difference (Microflown) of the temperature distribution of both the sensor-wires. When a flow is applied, the temperature of the wire (T_w) will drop because the convective heat loss increases.

$$T_w - T_f = \frac{P}{\pi l_c k_f (A + B\sqrt{v})} \tag{212}$$

Using k_f as the coefficient of thermal conductivity of the fluid, A and B are arbitrary constants, v represents the fluid velocity, P the dissipated power in the wire, T_f represents the fluid temperature, and l_c is a characteristic length of the channel (for a tube this is the inner diameter). The temperature distribution in the upstream direction of the flow (i.e. the x-direction) for static flow can be found from [1]:

$$T(x_{upstream}) = (T_w - T_f)\exp(x/l_{c1})$$
$$T(x_{downstream}) = (T_w - T_f)\exp(x/l_{c2})$$
$$with$$
$$l_{c1,c2} = \frac{2\frac{k}{\rho c}}{v \pm \sqrt{v^2 + 4\left(l_c \frac{k}{\rho c}\right)^2}} \tag{213}$$

Using ρ as the fluid density and c as the fluid heat capacity.

Model

Fig. 159 illustrates the principle of the flow sensor. Two hot wires (resistors) are located in the middle of the flow channel, one upstream and the other downstream the flow. The resulting temperature distribution caused by this flow is sensed with the same wires. The wires are located on supporting beams that penetrate the flow channel in the x-y plane.

DC flowsensor

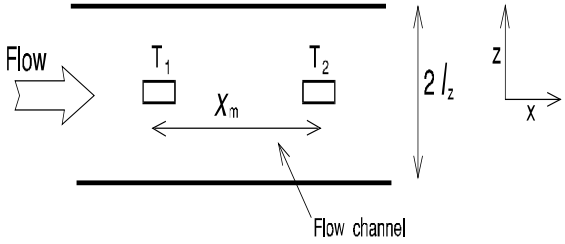

Fig. 159: The flow is measured by its influence on the temperature distribution of the wires.

In the model proposed by Lammerink et al, the temperature distribution in the fluid is assumed to be linear in the *z* direction and constant in the *y* direction [1].

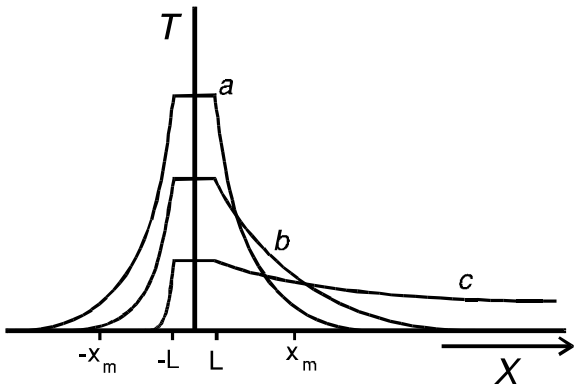

Fig. 160: Temperature distribution of only one hot wire in the middle of the channel as a function of the position x. The wire is from x=-L to x=L. a) v = 0; b) v= medium; c) v = high.

<u>Conduction:</u> At zero flow rate, no convection exists in the flow channel, and the heat generated by the wires will be transferred only by the axial and tangential conduction through the fluid and by the conduction through the wire support to the flow channel walls. The temperature distribution along the *x*-axis will typically posses an exponential behaviour as indicated by Eq. (213), Fig. 160 this distribution is plotted for zero flow in curve a.

Convection: In Fig. 161 the result of a flow, the common cooling of the wires is plotted Eq. (212). Clearly, the temperature drop is not depending on the direction.

In a stationary situation, the incoming heat at a certain point in the fluid must be equal to the outgoing heat. The heat is transported by conduction in the fluid and supporting beams and by convection through the thermal mass of the fluid. Ultimately, the heat is transported to the walls of the flow channel. A heat balance equation results in a differential equation for T in x. The temperature distribution for three different flow velocities is given in Fig. 160 [4].

The temperature distribution of both wires is found by taking a linear combination of both. Now the temperature is known as function of x direction and velocity, it is possible to generate a plot of the average (common) temperature of both wires and their temperature difference.

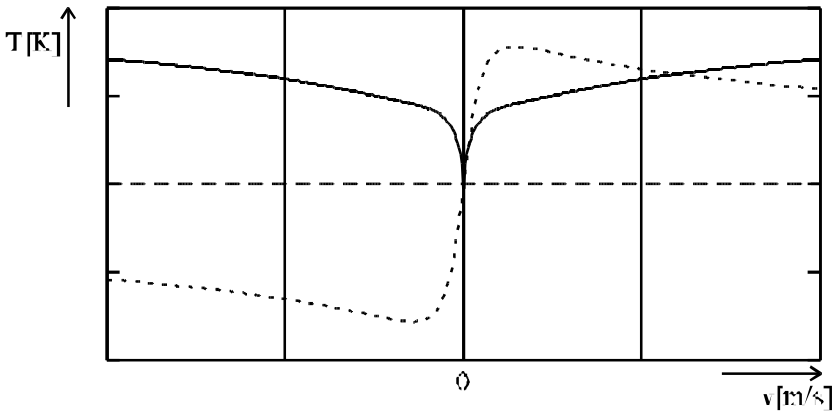

Fig. 161: The differential (dashed line) and common (solid line) temperature of both hot wires as a function of the velocity v. The common signal has been inverted to agree with the experimental data.

Fig. 161 is a result of the model. It should be noted that the constants A and B of Eq. (212) have been varied to fit the measured data from Fig. 163 As can be observed, the common temperature does not reveal any information concerning the flow direction. However, the differential output does give this information and improves the sensitivity and stability for low flows.

Electronic Circuit

The electronic circuit is shown in Fig. 162. It is build around the resistors R4&R5, which represent the flow sensor. The resistors R1&R2 represent a dummy flow sensor.

The circuit is fed with a constant voltage supply. R9&R8 and R10&R11 divide the power voltage supply, the capacitor provides a noise reduction so that the DC voltage on both the basis of Q3 and Q4 is “clean”. Due to the constant voltage on both basis the voltage over R4&R5 and R1&R2 is also of a constant value.

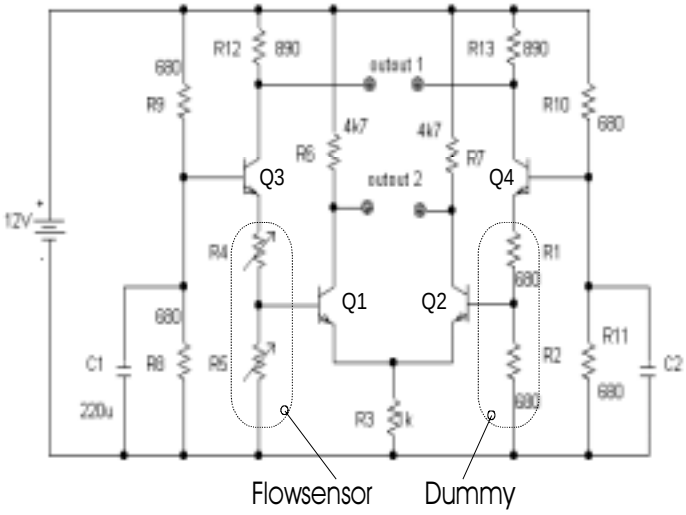

Fig. 162: Electric circuit for measuring the common and resistances of the Microflown.

If R4&R5 drop in value the current will increase and the voltage over R12 will increase. The dummy resistors R1&R2 will not drop in value and therefore the voltage over R13 remains constant. On “output 1” a signal representing the average cooling down of the flow sensor resistors R4&R5 can be found (the anemometer output).

The differential resistance variation of R4&R5 is measured with the differential amplifier that is created with R3, Q1 and Q2. The “mass flow sensor” output therefore can be found on “output 2”.

The noise that is generated in resistor R3 will be a common signal on “output 2”, the use of a differential amplifier therefore will result in a lower noise output.

Measurements

The flowsensor is can also be used as a Microflown, the corner frequency measured reaches the one Kilohertz. In the use of a flow sensor, this implies a response time in the order of milliseconds.

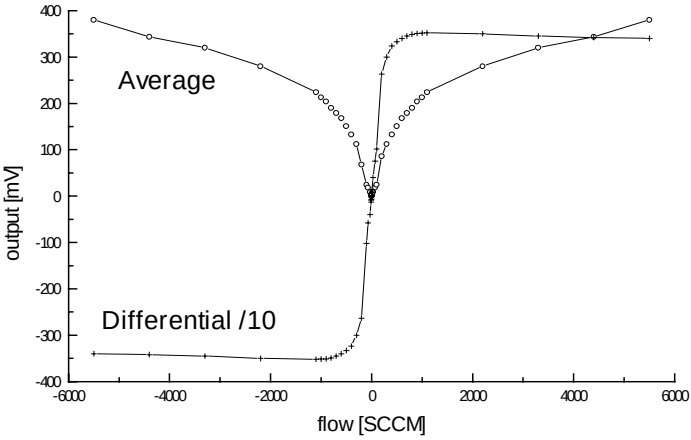

Fig. 163: Differential and common output signal of the sensor.

In Fig. 163 the temperature response of the sensor for flows up to 6000 SCCM is plotted. The diameter of the channel in which the sensor was inserted is ca. 1cm^2. The average (i.e. common) signal data has been fitted with Eq. (212) (solid line in Fig. 161) and it shows a reasonable resemblance. The differential output signal of the sensor has been divided by 10 to adjust for the difference in amplification between the differential and common output signal from the electronic circuit.

Discussion

In this paper it is shown that it is possible to measure a bi-directional flow with a large dynamic range. A simplified model shows a remarkable

qualitative resemblance with the measured data. The model has not yet been used to test the quantitative behaviour. The directivity of the differential part has a cosine shape. The anemometer however has no cosine shaped directivity. At higher velocities the plus or minus can only be found by the (saturated) differential signal.

Constant temperature principle

The sensitivity of the differential output drops due to the cooling of the complete device see Eq. (212), (213) and Fig. 160. If the sum temperature of both wires is kept constant the sensitivity of the differential signal will not drop.

The following circuit can achieve this. A feedback loop will provide a zero voltage difference at the input of the operational amplifier. The sum of the resistances of the Microflown will therefore kept equal to the sum of R4, R5 and R6. If, due to an airflow the resistance value of the Microflown drops, the voltage at the negative input of the amplifier drops. The output therefore will rise and more power will be dissipated in the Microflown. It therefore will rise in temperature, which will lead to an increase in resistance value. This process will go on until (sum) resistance of the Microflown equals the sum of R4, R5 and R6. R1 is used to start up the circuit.

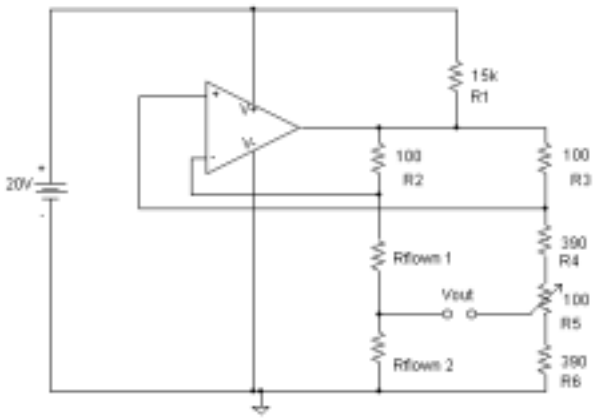

Fig. 164: A circuit that will keep the total temperature of the Microflown constant and is able to readout the differential temperature.

The response of the Microflown is shown in Fig. 165. As can be seen, the response of the Microflown in the constant temperature mode is an invertable function.

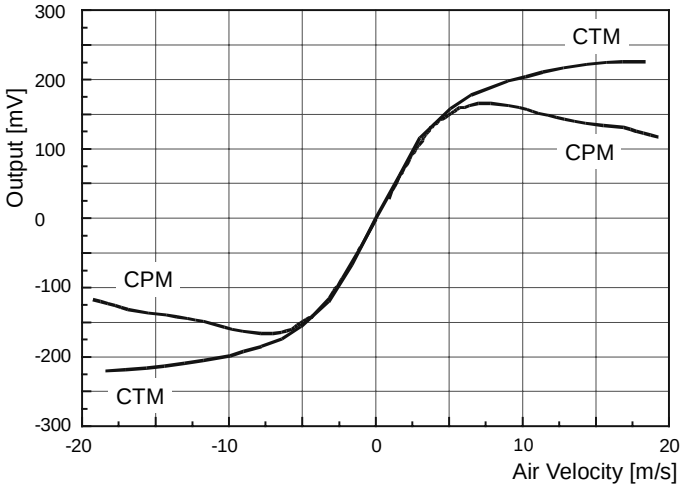

Fig. 165: The response of a Microflown in constant power mode (CPM) and in constant temperature mode (CTP) as function of the air velocity.

At a low velocity the voltage over the Microflown is about 6V and the sensitivity in the linear region is 40mV/ms^{-1}. The sensitivity of the Microflown is thus ½ $E \times \Delta R/R = 3 \times \Delta R/R = 40\text{mV/ms}^{-1} \rightarrow \Delta R/R = 13.3‰/\text{ms}^{-1}$. This value is in great resemblance with the sensitivity that was measured in the standing wave tube and anechoic room, see chapter 4, Fig 4.13.

References

[1] T.S.J. Lammerink et al, “Micro Liquid Flow Sensor,” *Sensors and Actuators A*, pp.37-38, 45-50, (1993).

[2] H.E. de Bree et al., “The μ-flown, A novel device measuring acoustical flows”, *Sensors and Actuators: A. Physical, volume SNA 054/1-3,* pp. 552-557, 1996

[3] C.G. Lomas, Fundamentals of hot wire anemometry, Cambridge University Press, Cambridge, 1986.

[4] H.E. de Bree et al., “The Two Sensor Microflown” *Eurosensors X*, Leuven, 1996

E4 A MICROFLOWN USED AS A SPIRIT LEVEL SENSOR

A Microflown can be used as a "spirit level"-sensor. The operation principle is still based on the temperature difference of two the identical heaters but now this difference is caused by buoyancy of air; no external flow is present. The sensor must therefore be packaged in a closed configuration. Heating as well as temperature sensing of the structures is carried out using temperature dependent platinum resistors. Theory describing the sensor is presented. First experiments show an adequate sensitivity though high accuracy operation is hampered by thermal drift.

Introduction

A spirit level (or vial) is an instrument that can detect if an object is placed horizontal. It is a widely used instrument that normally consists of an air bubble in a fluid. In Fig. 166 the two most common realisations are shown. The accuracy of these devices is about 2 to 30 arc-minutes. Various implementations of vials have been investigated in the past, see e.g. [1] and [2]. Although for most applications bubble vials are the tools of first choice some applications may require or benefit from small sized, solid state level sensors.

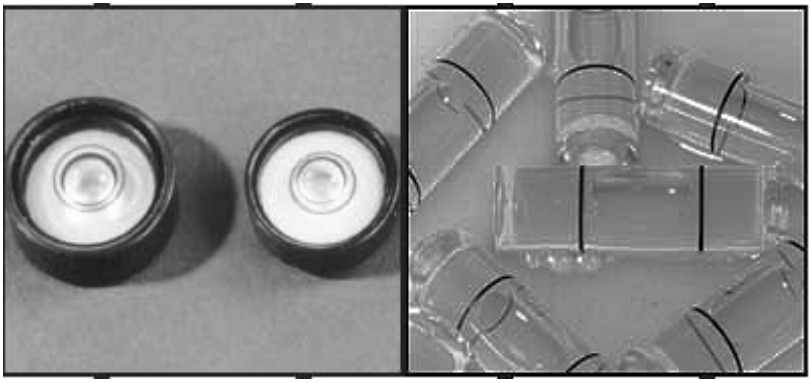

Fig. 166: Left: circular vials, right tubular vials

The vial discussed here consists of two heaters with platinum wires on top. These wires form resistors that are used to generate heat electrically. Simultaneously the resistors are used as temperature sensors exploiting the temperature resistance effect. Heat induced self-flow (or buoyancy) of the heated wires will cause a temperature difference of the two wires. This temperature difference is resolved by the temperature dependence of the resistors resolving in an output voltage deviating from zero (horizontal orientation) and a few tenth of a volt for none-level orientations. The realisation is well known: the sensing element is the same as that of a massflow sensor [3], a Microflown, or even an accelerometer [4]. For the latter two patents have been filed recently. It is quite remarkable that with only two heated wires, but in different set-ups it is possible to detect angle, velocity, or acceleration.

Operation principle

The principle, on which the present sensor is based, is the buoyancy, i.e. a combined presence of a fluid density gradient and a body force proportional to density. See e.g. [8]. In the present situation, the body force is the gravitation, whereas the density gradient is due to the temperature gradient, caused by the heating.

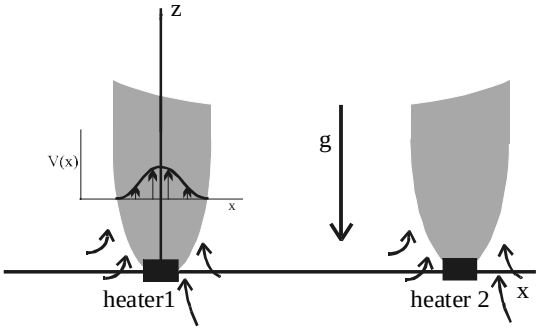

Fig. 167: Schematic of the geometry under consideration

Measurements

Some preliminary measurements demonstrate the operation principle of the level-sensor. From the temperature dependence of the resistive heaters the temperature difference can be detected. The elements are incorporated in a Wheatstone bridge, see Fig. 168, to obtain a high common signal rejection. Resistor R1 is fixed, R2 is adjustable to be able to zero the output voltage U_{out}. The resistance values of the heaters are denoted as R_{h1} and R_{h2}. The current through the heaters is 2mA, which gives a heat generation of 5.8mW. Their spacing is 100µm. The structure is placed in a small box to prevent any forced convection. To prevent air-velocity-temperature effects the electronic circuit is encapsulated as well.

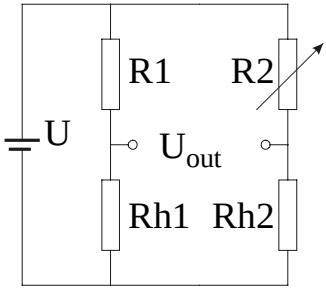

Fig. 168: Electronic circuit with R1=390Ω, R2=0-1kΩ and Rh1≈Rh2≈350Ω and U=3V.

With a simple set-up the plane parallel to the beams is ramped up from horizontal to 90 degrees and to minus 90 degrees. For each angle the mean value of 100 measurement points is plotted in Fig. 169. The standard deviation of the measurements was smaller than 1μV and therefore error bars are omitted in the graph.

The sensitivity of the level sensor is highest around the horizontal position, about 3μV/degree. The solid line is a fit of the measurement points using a least mean squares fit to a sine function.

From the difference in voltage drop over the both resistors we calculated the temperature difference of the beams (in vertical position) to be on the order of 50mK. During experiments we noted a clear drift of the output voltage on the order of 10μV limiting the accuracy of the level-sensor to 3 degrees around the horizontal position. We expect to be able to increase the accuracy by at least one order by using more advanced measurement methods. E.g. using AC signals drift signals can be considerably reduced.

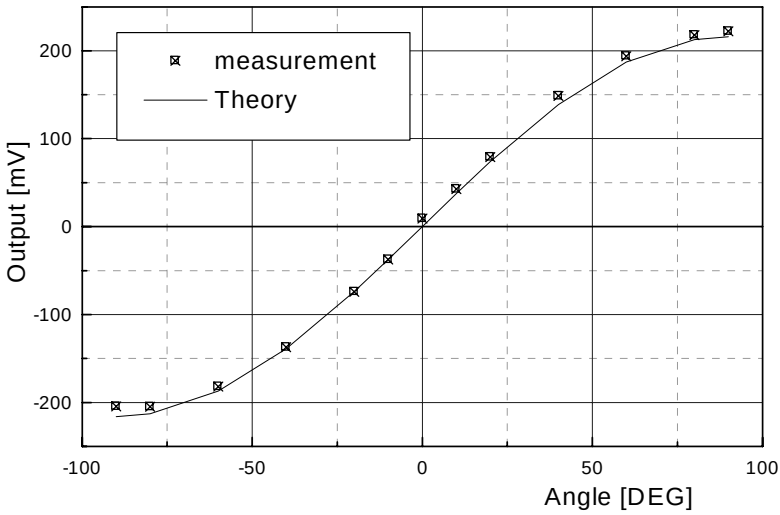

Fig. 169: Output voltage versus tilt.

Conclusions

A solid state level-sensor based on a Microflown technology has been presented. Experiments demonstrating the viability of the sensor are included. Although accuracy was hampered by drift we expect that large improvements can be obtained using different measurement techniques. Owing to silicon micro machining techniques these sensors could be low-cost alternatives to more accurate and expensive level sensors.

References

[1] Raatikainen P, Kassamakov I, Kakanakov R, Luukkala M, “Fiber-optic liquid-level sensor”, *Sensors and Actuators A-physical*, 58: (2) 93-97 FEB 1997

[2] Werthschutzky R, Hagist K, “Level Sensor with digital signal-processing”, technisches messen, 62: (11) 416-423 NOV 1995

[3] T.S.J. Lammerink et al, “Micro Liquid Flow Sensor,” *Sensors and Actuators A*, pp.37-38, 45-50, (1993).

[4] A. Leung, J. Jones, E. Czyzewska, J. Chen and M. Pascal, "Micromachined Accelerometer With No Proof Mass", IEDM, Washington, DC, December 7-10, 1997, p899-902.

[5] Fundamentals of hot wire anemometry, C.G.Lomas, *Cambridge University Press*, Cambridge, 1986

[6] R.Aigner et al, "SI-Planar- Pellistor Designs for temperature modulated operation", ‘95-Eurosensors IX, 213-PD5

[7] Yang et. al., Monolithic flow sensor for measuring millimeter per minute flow, *Sensors and Actuators A*, 33, 1992, 143-153

[8] Fundamentals of heat and mass transfer, F.P.Incropera, D.P. deWitt, *John Wiley & Sons*, New York, 1990

E5 THERMOFLOWN

Fig. 170: A Thermoflown (thermophone or thermal loudspeaker) that consists on 12 discrete Microflowns. With this unit we found out that Microflowns can produce sound (Doekle Yntema).

Thermoflown

A Microflown is an acoustic sensor (microphone) that is capable to measure particle velocity in stead of sound pressure. It is a modulator type of sensor; a thermal energy flow is modulated by sound (the particle velocity) and two temperature sensors detect this. Modulator type of sensors are normally not reversible which means that the sound energy (or better the sound signal) can modulate the energy flow in the sensor but modulating the energy flow will not generate sound.

Although the Microflown is a modulator type of sensor, it is able to produce sound. The sound that is generated by the Microflown is caused by temperature variations of the sensor-wires. These variations cause a pressure fluctuation that can be perceived as sound.

The Microflown consist on two very thin (300nm) wires and due to the physical dimensions of the wires, high frequency temperature variations (up to about 10kHz) can be reached. If the device is used as an acoustic sensor it displays two corner frequencies, one is caused by the heat capacity of the sensors and the other is due to diffusion effects. When used as a loudspeaker, the diffusion corner frequency will not be noticed. The diffusion effects between the two wires cause this corner frequency and only one wire is needed for the loudspeaker application. The other corner frequency that is caused by the thermal capacity of the sensor will still be noticeable. This corner frequency is in the order of 5kHz to 10kHz.

To use it as a thermal loudspeaker the two wires are switched in series. A varying supply current $I(t)=I\ sin(\omega t)$ voltage causes a heat development in the wire of $Q=Ri^2sin^2(\omega t)= ½(Ri^2(1-cos2\omega t))$. This heat variation causes a temperature variation directly surrounding the wire. The expansions and contractions that are caused due to this are observed as sound.

A single Microflown generate sound levels that are too small to perceive. Therefore multiple (250) Microflowns are constructed in such way that the effective length of the wires increased to 25cm, chapter D4. Furthermore an initial DC current I_0 is applied so that the double frequency term reduces: $Q=R(I_0+isin\omega t)^2=R(I_0^2+½i^2)+2R\ \ I_0isin\omega t-½Ri^2cos2\omega t$

The frequency response is shown in Fig. 171. A 1.25W DC and a 0.5mW AC power was submitted.

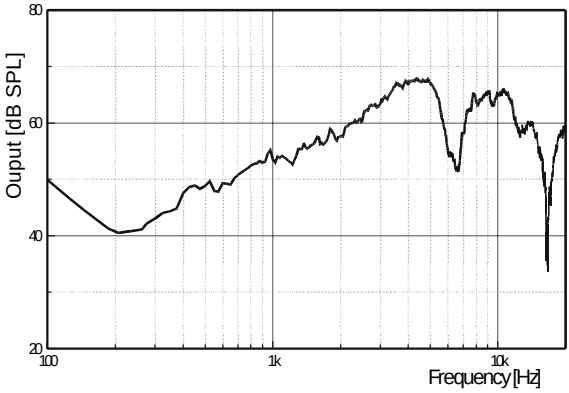

Fig. 171: Frequency response of the thermal loudspeaker (input was 0.5mW white noise).

When no DC power is submitted, a output signal with a double frequency is observed, see Fig. 172. The signal was a 50mW sine wave with frequency 3kHz. If the DC power (1.25W) is switched on, the double frequency disappears and the single 3kHz can be perceived. In the latter experiment, a 0.5mW power was submitted. See Fig. 173.

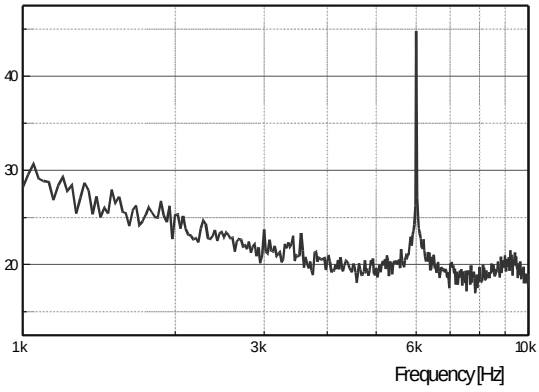

Fig. 172: Output due to a 50mW sine wave input with frequency 3kHz. Only the double frequency is observed.

Thermoflown

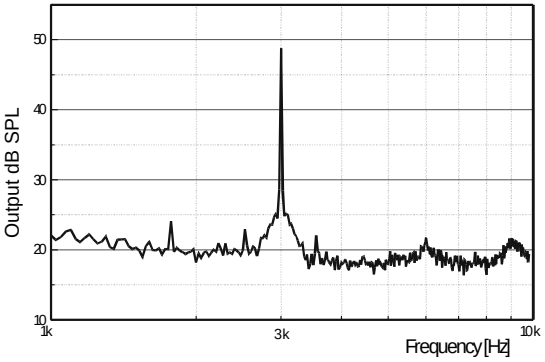

Fig. 173: Output due to a 0.5mW sine wave input with frequency 3kHz. No double frequency is observed.

The idea to use a single wire to generate sound is not new, it is known as a thermophone, see [1-3]. However micromachining construction possibilities (the possibility to create very thin wires) may enhance the sound quality of these old techniques.

The Thermoflown is also realised as miniature headphone [1].

References

[1] D.R. Yntema, Report of a thermal loudspeaker based on Microflown technology, intern report.

[2] A.B. Wood, A textbook of sound, 1964 (first published 1930).

[3] P. de Lange, Proc. Roy. Soc. 91, p.239, April 1915.

APPENDIX I: SOLVING THE WAVE EQUATION FOR A SPHERICAL WAVE

The one-dimensional wave equation yields:

$$\frac{\partial^2 p(t,x)}{\partial x^2} - \frac{1}{c^2}\frac{\partial^2 p(t,x)}{\partial t^2} = 0 \tag{214}$$

This wave equation must be satisfied by acoustic waves propagating in the medium. However, in order to find solutions to this equation the form that the sound field must take must be specified in more detail. Boundary conditions must be specified in order to find the form of the sound field.

As an example the (three-dimensional) wave equation will be solved for a spherical sound field radiated from a point source. The three-dimensional expansion of the wave equation is given by:

$$\left(\frac{\partial^2}{\partial x^2} + \frac{\partial^2}{\partial y^2} + \frac{\partial^2}{\partial z^2}\right)p - \frac{1}{c^2}\frac{\partial^2 p}{\partial t^2} = \nabla^2 p - \frac{1}{c^2}\frac{\partial^2 p}{\partial t^2} = 0 \tag{215}$$

Since the radiation from the point source is spherically symmetric the sound pressure p depends only on r, with $r = \sqrt{x^2 + y^2 + z^2}$.

So the wave equation can be written as a function of r instead of x, y and z. At first:

$$\frac{\partial r}{\partial x} = \frac{\partial}{\partial x}\sqrt{x^2 + y^2 + z^2} = \frac{2x}{2\sqrt{x^2 + y^2 + z^2}} = \frac{x}{r}$$

and

$$\frac{\partial^2 r}{\partial x^2} = \frac{\partial}{\partial x}\frac{x}{r} = \frac{1}{r}\frac{\partial}{\partial x}x + \frac{\partial}{\partial r}\frac{x}{r}\frac{\partial r}{\partial x} = \frac{1}{r} + \frac{-x}{r^2}\frac{\partial r}{\partial x} \tag{216}$$

$$= \frac{1}{r} + \frac{-x}{r^2}\frac{x}{r} = \frac{1}{r}\left(1 - \frac{x^2}{r^2}\right)$$

The x part of $\nabla^2 p$ can be written as:

Appendix I

$$\frac{\partial^2 p(r)}{\partial x^2} = \frac{\partial}{\partial x} \cdot \frac{\partial p}{\partial x} = \frac{\partial}{\partial x} \cdot \left(\frac{\partial p(r)}{\partial r} \frac{\partial r}{\partial x} \right) = \frac{\partial}{\partial x} \cdot \left(p'(r) \frac{\partial r}{\partial x} \right)$$

$$= \left(\frac{\partial}{\partial x} p'(r) \right) \frac{\partial r}{\partial x} + p'(r) \frac{\partial}{\partial x} \left(\frac{\partial r}{\partial x} \right) = \frac{\partial}{\partial r} p'(r) \frac{\partial r}{\partial x} \frac{\partial r}{\partial x} + p'(r) \frac{\partial^2 r}{\partial x^2} \quad (217)$$

$$= p''(r) \left(\frac{\partial r}{\partial x} \right)^2 + p'(r) \frac{\partial^2 r}{\partial x^2} = p''(r) \frac{x^2}{r^2} + p'(r) \frac{1}{r} \left(1 - \frac{x^2}{r^2} \right)$$

Likewise the y and z part can be written as:

$$\frac{\partial^2 p(r)}{\partial y^2} = p''(r) \frac{y^2}{r^2} + p'(r) \frac{1}{r} \left(1 - \frac{y^2}{r^2} \right)$$

$$\frac{\partial^2 p(r)}{\partial z^2} = p''(r) \frac{z^2}{r^2} + p'(r) \frac{1}{r} \left(1 - \frac{z^2}{r^2} \right) \quad (218)$$

The sum of the three:

$$\nabla^2 p = \frac{\partial^2 p(r)}{\partial x^2} + \frac{\partial^2 p(r)}{\partial y^2} + \frac{\partial^2 p(r)}{\partial z^2} =$$

$$= p''(r) \frac{x^2 + y^2 + z^2}{r^2} + p'(r) \frac{1}{r} \left(3 - \frac{x^2 + y^2 + z^2}{r^2} \right) \quad (219)$$

$$= p''(r) + \frac{2}{r} p'(r)$$

The latter equals:

$$\nabla^2 p = \frac{1}{r} \frac{\partial^2}{\partial r^2} \left(r \cdot p(r) \right)$$

$$\frac{1}{r}\frac{\partial^2}{\partial r^2}\left(rp(r)\right)=\frac{1}{r}\frac{\partial}{\partial r}\frac{\partial}{\partial r}\left(r\cdot p(r)\right)=\frac{1}{r}\frac{\partial}{\partial r}\left(p(r)+r\frac{\partial p(r)}{\partial r}\right)$$
$$=\frac{1}{r}\left(\frac{\partial}{\partial r}p(r)+\frac{\partial p(r)}{\partial r}+r\frac{\partial^2 p(r)}{\partial r^2}\right)=\frac{1}{r}\left(2\frac{\partial}{\partial r}p(r)+r\frac{\partial^2 p(r)}{\partial r^2}\right) \quad (220)$$
$$=p''(r)+\frac{2}{r}p'(r)$$

So the wave equation for spherically symmetric wave propagation is given by:

$$\nabla^2 p(r)-\frac{1}{c^2}\frac{\partial^2 p}{\partial t^2}=\frac{1}{r}\frac{\partial^2(r\cdot p)}{\partial r^2}-\frac{1}{c^2}\frac{\partial^2 p}{\partial t^2}=0$$
$$\leftrightarrow \quad (221)$$
$$\frac{\partial^2(r\cdot p)}{\partial r^2}-\frac{1}{c^2}\frac{\partial^2(r\cdot p)}{\partial t^2}=0$$

Since the new function $r\cdot p$ should obey the wave equation Eq. (2.13), of which the solution is of the form $Ae^{i(kx\pm\omega t)}$, the pressure p should be a harmonic outwards-travelling wave proportional to $1/r$:

$$p(r,t)=Re\left\{\frac{Ae^{i(\omega t-kr)}}{r}\right\} \quad (222)$$

Substitution of Eq. (2.14) in Eq. (2.13) shows that this function of the sound pressure obeys the wave equation:

Appendix I

$$\frac{1}{r}\frac{\partial}{\partial r}\frac{\partial r\cdot p(r,t)}{\partial r}=\frac{1}{r}\frac{\partial}{\partial r}\frac{\partial}{\partial r}Ae^{i(\omega t-kr)}$$
$$=\frac{1}{r}\frac{\partial}{\partial r}\left(-Ae^{i(\omega t-kr)}k\right)=\frac{Ae^{i(\omega t-kr)}k^2}{r}=k^2p(r,t)$$
$$and$$
$$-\frac{1}{c^2}\frac{\partial^2}{\partial t^2}\left(r\cdot p(r,t)\right)=-\frac{1}{c^2}\frac{\partial}{\partial t}\frac{\partial}{\partial t}Ae^{i(\omega t-kr)} \tag{223}$$
$$=-\frac{1}{c^2}\frac{\partial}{\partial t}Ae^{i(\omega t-kr)}i\omega=-\frac{1}{c^2}Ae^{i(\omega t-kr)}i^2\omega^2$$
$$=-\frac{1}{c^2}Ae^{i(\omega t-kr)}i^2\omega^2=\frac{\omega^2}{c^2}p(r,t)=k^2p(r,t)$$

The linearised equation of momentum conservation (see chapter 2) can be used to find the particle velocity that is associated with the sound pressure:

$$u(x,t)=\frac{-1}{\rho_0}\int\frac{d}{dx}p(r,t)dt=\frac{1}{\rho_0}\int\frac{d}{dx}\frac{Ae^{i(\omega t-kr)}}{r}dt$$
$$=\frac{-1}{\rho_0}\int-\frac{Ae^{i(\omega t-kr)}}{r^2}-\frac{Ae^{i(\omega t-kr)}}{r}ikdt=\frac{-1}{\rho_0}\int\left(\frac{1}{r}+ik\right)\frac{-Ae^{i(\omega t-kr)}}{r}dt \tag{224}$$
$$=\frac{1}{\rho_0}\left(\frac{1}{r}+ik\right)\frac{Ae^{i(\omega t-kr)}}{r}\frac{1}{i\omega}=\frac{A}{i\omega\rho_0}\left(\frac{1}{r}+ik\right)\frac{e^{i(\omega t-kr)}}{r}$$

The specific acoustic impedance as a function of the radial distance:

$$z(r)=\frac{p(r,t)}{up(r,t)}=\frac{A\frac{e^{i(\omega t-kr)}}{r}}{\frac{A}{i\omega\rho_0}\left(\frac{1}{r}+ik\right)\frac{e^{i(\omega t-kr)}}{r}}=\frac{i\omega\rho_0}{\left(\frac{1}{r}+i\frac{\omega}{c}\right)}=\frac{i\frac{\omega}{c}c\rho_0 r}{\left(1+i\frac{\omega}{c}r\right)}=c\rho_0\left(\frac{ikr}{1+ikr}\right) \tag{225}$$

APPENDIX II: SOUNDCARD BASED DUAL CHANNEL ANALYSER FOR THE PU PROBE

The software is programmed in MATLAB® around a Graphical User Interface for convenience in usage, and because MATLAB® is widely used and is an easy program language so that users are able to modify the software to their demands. The program is capable of working in three modes: Instantaneous, a measurement for 30 seconds and data processing from a wave file.

The instantaneous mode is very useful in examining the acoustical situation. In the instantaneous mode it is possible to compute and show various windows containing:

- the auto spectra of the pressure and particle velocities.
- the coherence between the two signals.
- the intensity (active, reactive, and the phase).
- the sound energy.
- the active and reactive intensity divided by the energy (indicating a net power transport velocity and reflection).
- the acoustical impedance (magnitude, real and imaginary part).

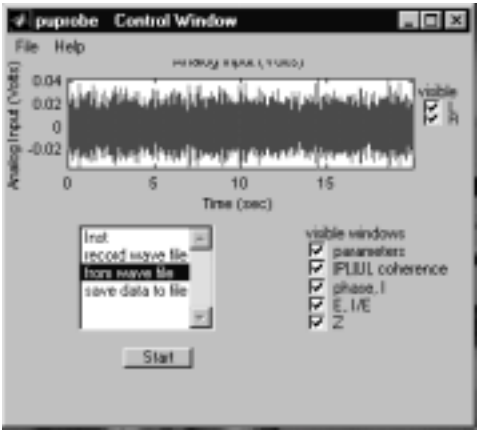

Fig. 174: The control window. In this window the signals as function of the time can be seen. This is useful as a first check if the measurement data is correct.

All axes can be chosen as linear or logarithmic scales and the vertical axis are by default in dB. Both the frequency spectrums in terms of the frequency as the spectrum in 1/3-octave bands can be displayed. Calculated spectra's can be saved to the workspace, or as MATLAB® .mat files and as ASCII files for further processing. It should be noted that the 1/3 octave band of 20kHz is an underestimation in case a sample frequency of 44.1kHz is used. This underestimation is due to the fact that the power is not know in the whole 1/3 octave band, and the A/D converter will not be less accurate above 20kHz. If sample frequencies of 48kHz (or higher if possible) are used, the 20kHz 1/3 octave band will be computed correctly.

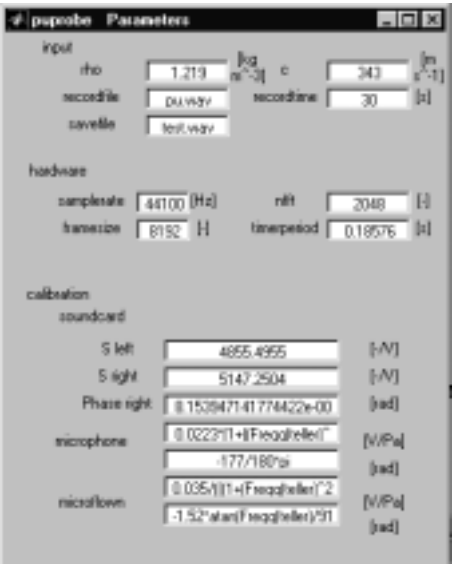

Fig. 175: In the parameter window all relevant data has to be filled in. Most significant is the possibility to correct the phase and amplitude response of the microphone, Microflown and sound card.

In the instantaneous mode it is not convenient to use large frames because of computing time and power, resulting in a small frequency resolution, the default size of the frame is set at 2048. For higher resolution it is advisable to save the signals into wave files so that they can be processed later with higher frequency resolution. We should note that a good frequency resolution is necessary if we would like to use the advantage of low frequency measurements, which is possible due to the

physics of the p-u probe. The size of frames for the Fast Fourier Transform can be altered according the wanted frequency resolution, and computation time (default 16834). By default a Hanning window is used for increasing the spectral resolution.

It is possible to record measurements using external hardware like external A/D converters connected to digital Soundcards, CD-Recorders, or DAT-recorders. This is also very convenient since most of these are rather mobile while measuring becomes rather easy and post processing can be automated with use of the available software.

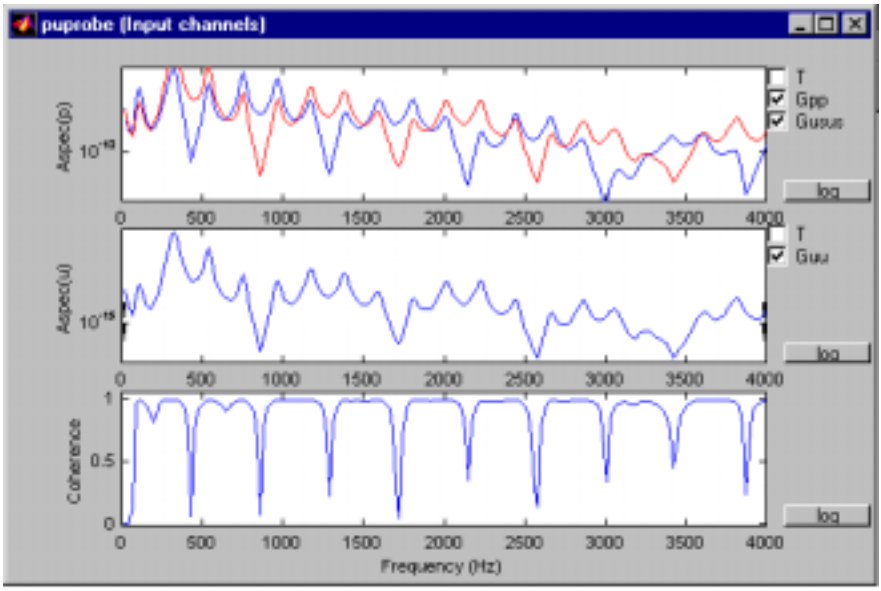

Fig. 176: The input window. The auto spectrum (phase and amplitude response corrected signals function of frequency) of both microphones. Upper window: auto spectrum of particle velocity (in Pa*) and sound pressure in Pa. Middle window: particle velocity (in m/s). Both windows can toggle to get 1/3-oct band information (T). The lower window displays the coherence. If this value is larger than 0.8 the measurement is valid. All frequency axis can be plotted linear or logarithmically.

Appendix I

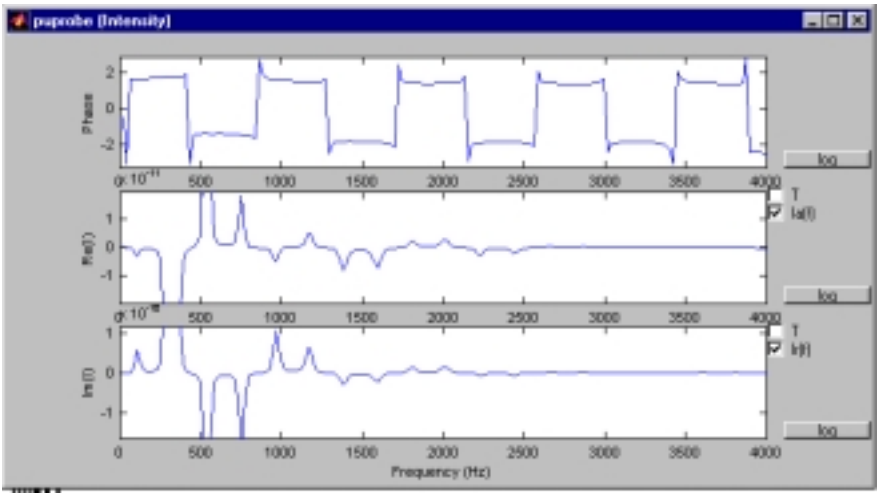

Fig. 177: The phase and intensity window. The phase between sound pressure and particle velocity is displayed in the upper window. This phase is also the phase of the intensity and impedance. The lower two windows are used to display the real and imaginary part of the intensity (cross spectrum).

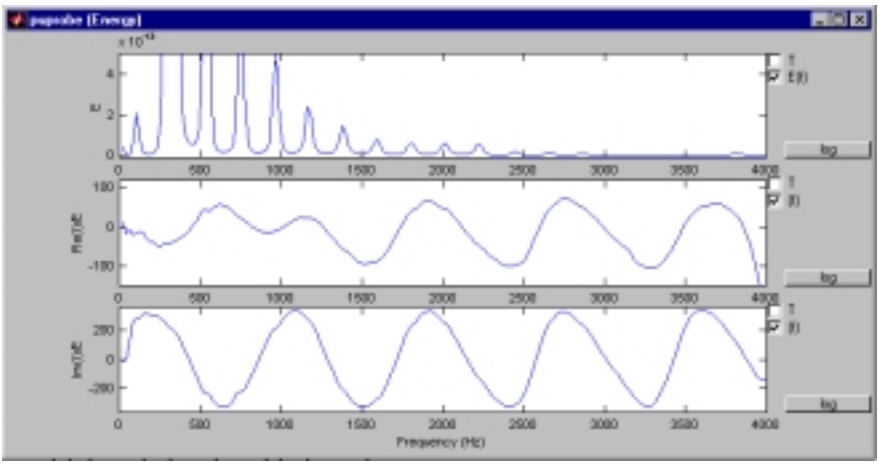

Fig. 178: The energy window. The energy of the sound wave is displayed in the upper window. If a sound wave is plane and no reflections are present, the intensity equals the product of the energy and the speed of sound. So the lower two windows reveal an “amount of reflection”.

Index

1

1/f-noise, 102
  measurement, 102
  pressure microphone, 59

3

3D Microflown, 244
3D pu probe
  experimental, 240
3D ultra miniature probe, 243

A

acoustic impedance, 15, 27, 54, 55, 269
acoustic input impedance of a horn, 272
A-weighing curve, 63, 120

B

backplate, 59
bandwidth, 59

C

calibration
  impedance tube, 299
  open window method, 219
  reverberant room, 219
calibration methods, 171
  An accurate model of the standing wave tube measurement, 178
  standing wave tube (SWT), 176
  The anechoic chamber, 172
  the long tube, 174
capacitive microphone, 58
capillary vent, 59
characteristic impedance, 54
Characteristics of a Microflown, 115
  Corner frequency curve, 118
  sensitivity curve, 116
  The Power Curve, 115
chemical etching, 90
condenser microphone, 58
conductive heat flow, 71
convective heat transfer, 71
cross-section of a condenser microphone, 58
cyanoacrylate, 95

D

damping
  free field methods, 283
  impedance tube methods, 284
  reverberant field method, 282
  the 2p and 2u method, 294
  the p/u method, 292
  the p·u method, 298
  the p-p method, 293
dicing of Microflowns, 93

E

ear, 43
electret microphone, 58
Electromagnetic microphones, 58
Equal loudness contours, 62
equation of mass conservation, 48
equation of momentum conservation, 49

F

figure of eight, 14
free field, 52, 54
frequency, 53
frequency response
  Microflown, 71
  pressure gradient microphone, 65

H

harmonic distortion, 60
human ear, 62

I

ICP probe
  BNC connector, 160
  frequency response / noise spectrum, 163
  ICP preamplifier, 161
  linearity, 165

phase response, 164
Polar pattern, 165
preamplifier, 161
the half-inch ICP probe, 160
infrasound array, 40

K

kinetic energy, 55

L

Loudness, 62

M

measurement results
acoustic impedanvce of a horn loudspeaker, 276
membrane, 58
membrane microphones, 57
Microflown, 12, 15, 69
amplitude of particle motion, 13
applications, 32
bridge type, 74
cantilever type, 74
construction methods, 82
dimensions, 14
directionality, polar patern, 15
high-end applications, 15
History, 17
ICP protocol, 27
measured temperature response, 98
package gain, 14, 25
parts, 14
photo first bridge type, 21
photo first cantilever type, 22
photo of bridge type, 85
photo of cantilever type, 84
photo of through the wafer type, 85
picture of cantilever type, 69
power dissipation, 15
size, 70
Symbol, 16
Technology History, 20
temperature distribution, 17
trough the wafer type, 74
micromachining, 86
microphone, 12, 15, 57
construction, 17
Microflown (velocity), 69
ribbon (velocity) microphone, 67
ultrasonic transduction (velocity), 68
micro-pipette, 80
microtechnology, 77
model of the Microflown
simple model, 70
modelling
analytical model, 133
corner frequeny as unction of the spacing, 153
diffusion corner frequency, 148
low frequency sensitivity (LFS), 138
Low frequency sensitivity as function of the spacing, 153
stationary situation, 134
temperature distribution, 133
temperature distribution around one wire, 139
temperature distribution due to convection for two heaters, 140
thermal capacity corner frequency, 149
thermal diffusion coefficient, 150
molecular mean free path, 53

N

nearfield effect, 51
nitride deposition, 88
noise levels (measured) of a half-inch p-p probe, 255
noise levels (measured) of a half-inch p-**u** probe, 254
noise properties
audio, 119
high-end audio, 129

Influence of the 1/f nosie (Audio), 125
measurement, 122
quantification, 119
telecom, 126
noise spectrum (measured) of a ½" ICP Probe, 250
noise spectrum (measured) of a GRAS Type 40AC, 249
noisefactor (Microflown), 121

O

omni-directional, 60
one-dimensional wave equation, 50

P

package gain, 72, 156
business cards, 158
half-inch ICP probe, 157
protecting cap, 156
packaging, 94
particle velocity, 16, 44, 53
ultrasonic transduction, 68
particle velocity level, 56
particle velocity microphone, 66
polar patern, 67
performance (Microflown), 121
photolithography, 89
polar pattern, 14
pressure gradient microphone, 64
pressure microphone, 60
polarisation voltage, 59, 60
potential energy, 55
pp probe, 205
drawbacks, 205
sound intensity, 204
p-p sound intensity method, 49
preamplifier
4mA ICP Preamplifier, 112
camparison, 113
CE gadget, 108
First realisation Gadget, 105
pressure microphone, 59
The Gadget, 104
preamplifiers, 28
CE-Gadget, 28
ICP, 28
phantom, 29
the Gadget, 28
pressure microphone, 57
pressure microphones, 46
pu probe, 206
calibration, 219
cross section, 218
design considerations, 217
directional characteristics, 207
frequency response Microflown, 229
half-inch probe, 216
half-inch sound intensity probe, 218
intensity measurements, 233
measurements, 227
photo first operational probe, 206
software, 222
the phase of the Microflown, 229

R

realisation of the 3-D ½" p-p probe, 239
realisation of the 3-D pu probe, 238
ribbon microphone, 67
RIE etching, 92

S

selfnoise, 59
Microflown, 73
sensitivity
Microflown, 72
pressure microphone, 59
separation (distance)
pressure gradient microphone, 65
signal to noise ratio
pp and pu probe, 247
theory, 101
sound, 43
Sound, 44
sound energy density, 15
Sound energy density, 55, 269
sound intensity, 15, 27, 54, 74, 199, 200

experimental, 208
formula, 204
phase mismatch of probes, 207
photo first probe, 28
Sound intensity, 55, 269
sound intensity level, 56
sound pressure, 44, 53, 57
Sound pressure, 16
sound pressure gradient, 63
sound pressure level, 56
specific acoustic impedance, 54, 55, 269
spherical sound field, 50
sputter deposition, 89
standard cleaning, 88
statistical data, 167

T

thermal noise
pressure microphone, 59
three-dimensional probe, 238
transducer, 12

U

u-u probe, 206
***u-u** sound intensity method*, 48
u-u sound measurement, 258

V

velocity microphone, 64
Microflown, 69
ribbon microphone, 67
ultrasonic transduction, 68
viscothermal effects, 40

W

wave equation, 47
wave number, 50
wavelength, 53
wind (influence of), 256
wobble motor, 78

BIOGRAPHY

Hans-Elias de Bree was born in 1969 in Soest, the Netherlands. He took the “long way” to the university meaning that he went from the technical school to the technical college and moved over after one year to the Technical University in Twente. Just before his first sabbatical leave to Indonesia he discovered the Microflown in 1994. After his return he graduated Electrical Engineering on low noise electronics in 1995.

Two years later he got his Ph.D. degree on the research efforts regarding the Microflown. From then he worked as senior researcher at the Mesa Research Institute on micro machined sound intensity probes. In June 2001 he will enjoy together with his girlfriend his second sabbatical leave sailing from The Netherlands to the Caribbean and (hopefully) back again.

Fig. 179: One of the first times that Inez and Hans-Elias are sailing with their boat.